Journal of Alloys and Compounds 509 (2011) 9105–9110

Contents lists available at ScienceDirect

Journal of Alloys and Compounds

journal homepage: www.elsevier.com/locate/jallcom

A facile method to synthesize high-quality ZnS(Se) quantum dots for photoluminescence

F.Y. Shen, Wenxiu Que*, X.T. Yin, Y.W. Huang, Q.Y. Jia

Electronic Materials Research Laboratory, School of Electronic and Information Engineering, Xi'an Jiaotong University, Xi'an 710049, Shaanxi, People's Republic of China

ARTICLE INFO

Article history:
Received 9 March 2011
Received in revised form 10 June 2011
Accepted 14 June 2011
Available online 21 June 2011

Keywords:
Oleylamine
Zinc sulfide
Quantum dot
Photoluminescence

ABSTRACT

Colloidal zinc sulfide (ZnS) quantum dots are synthesized by a solvothermal route from $Zn(Ac)_2{\cdot}2H_2O$, sulfur powder and oleylamine at 120–240 °C. Microstructural, morphological, and optical properties of the as-synthesized ZnS quantum dots are characterized by X-ray diffraction analysis, transmission electron microscopy, UV–vis absorption spectroscopy, and photoluminescence spectroscopy. Results indicate that the obtained ZnS quantum dots distribute uniformly, the particle size is in the range between 1.7 nm and 3.1 nm, and the band gap decreases from 4.16 eV to 3.90 eV with an increase of the particle size. The size-dependent photoluminescence exhibits a strongly broadened peak accompanied by a pronounced blue-shift. It is also found that the size of the ZnS nanocrystals can be effectively controlled by adjusting synthesis temperature. It is shown that the present method is also applicable to synthesize other binary II–VI semiconductor materials, such as ZnSe quantum dots.

1. Introduction

Semiconductor nanocrystals, also termed quantum dots (QDs), have been attracting a great deal of attention in recent years due to their technical applications, such as biomedical labeling, light-emitting diodes, photocatalysis, solar cells, lasers, and sensors [1–6]. Therefore, II–VI semiconductors, such as CdSe, CdTe and their alloys, have been intensively studied in the form of size-, shape- and stoichiometry-controlled during the past decade [7–9]. However, in view of recent environmental regulation, the intrinsic toxicity of cadmium brings a doubt on the future applicability of the cadmium compounds despite of their great optical and electrical properties. Thus, several Cd-free alternative materials have been proposed including III–V semiconductor nanocrystals and transition-metal-doped ZnS and ZnSe QDs [10–12].

ZnS, as a kind of broad-band semiconductor material, has a wide band gap of 3.68 eV for the cubic blende phase and 3.91 eV for the hexagonal wurtzite phase at room temperature, respectively [13]. As a nontoxic semiconductor material, it shows strong photocatalysis ability and is widely used in light-emitting and microcircuit devices. ZnS layer can inhibit a recombination of the excited electron at the electrode/electrolyte interface and it can be also used as a passivation layer for CdS or CdSe to enhance the performance of the photoelectrode [14,15]. Especially, the energy conversion efficiency of TiO_2/MPTMS/CdSe cell can increase from 1.80% to 2.29% due to the introduction of the ZnS passivation layer [16]. It has been also shown that the ZnS layer cannot only improve the optical properties, but also protect below layers from corrosion by the liquid electrolyte. It has been demonstrated that the properties of the ZnS nanocrystal depend on the size and morphology largely.

Many methods have been developed to obtain uniform II–VI nanocrystals, including vapor deposition process [17], hydrothermal synthesis [18], solvothermal synthesis [19] and sol–gel method [20]. In particular, there are very recent works reporting the synthesis of CdSe and ZnTe nanocrystals in solid templates by using glass as a matrix [21,22], in which the fusion is carried out at a high temperature. As reported in Ref. [23], a reliable synthesis route for high-quality colloidal NCs of the controlled size and shape can be used to synthesize most binary and some ternary semiconductors, but not much attention has been paid to the blende-type ZnS QDs. Furthermore, ZnS crystalline colloidal arrays were synthesized by using thioacetamide and zinc–nitrilotriacetate [24]. Zinc blende ZnS nanowires were synthesized by using a hexagonal liquid crystal as template [25]. Mesostructured wurtzite ZnS–nanowires were synthesized by using a mild-solution reaction with different amines [26]. Tiny wurtzite ZnS nanoparticles were synthesized at 150 °C by a solution chemistry approach [27], and a ligand-controlled synthesis at elevated temperatures higher than 150 °C was also developed [28,29]. In addition, highly luminescent $CuInS_2$/ZnS core/shell nanocrystals were synthesized in octadecene, dimethylformamide and toluene [30]. However, all these synthesis methods are either complicated or high cost, or due to toxic precursors. Herein, we present a synthesis method for the intrinsic ZnS semiconductor QDs and characterize the morphology, absorption, and

* Corresponding author. Tel.: +86 29 82668679; fax: +86 29 82668794.
E-mail address: wxque@mail.xjtu.edu.cn (W. Que).

0925-8388/$ – see front matter © 2011 Elsevier B.V. All rights reserved.
doi:10.1016/j.jallcom.2011.06.061

photoluminescence properties. To the best of our knowledge, the ZnS QDs synthesized from oleylamine has been little reported so far. Our method for synthesis of the ZnS QDs is simple and low-cost. Besides, the as-synthesized nanoparticles are uniform and the particle size can be controlled by adjusting reaction temperature. It is found that the synthesis route is versatile to the large-scale production and suitable for preparing other binary or ternary semiconductor materials.

2. Materials and methods

Zinc acetate dihydrate ($Zn(Ac)_2{\cdot}2H_2O$), sulfur (S) powder, selenium powder, hexane, and ethanol were purchased from China National Medicines Corporation Ltd. Oleylamine (OLA; 90%) was purchased from Jingchun Reagent Co. Ltd., Shanghai. All the chemicals used in our experiment were received from commercial products without any further purification and they are analytical grade reagents.

A flask was used as reaction vessel in our experiment. Firstly, 0.439 g (2 mmol) of $Zn(Ac)_2{\cdot}2H_2O$, and 10 mL of oleylamine were mixed together in the flask at room temperature, and then the mixed solution was heated to 80 °C with a magnetic stirring and maintained for 30 min until the Zn salt was completely dissolved in the solvent. Thus, the transparent solution was obtained. Secondly, 0.064 g (2 mmol) of S powder was dissolved in the previous solution. The resulting mixture was then heated to 120–240 °C and maintained for 30 min with vigorous magnetic stirring to form a dispersive mixture. It was noted that the color of the mixed solution changed from colorless to pale yellow and then to dark yellow with the addition of the S powder. After the flask was cooled to room temperature, the products were slowly precipitated with the addition of the anhydrous ethanol. The mixture was centrifuged and the supernatant was decanted. Then the sediment was dispersed in hexane. The process of the dispersion and centrifugation was repeated for 3 times with hexane and ethanol to remove the rest precursor. Finally, the ZnS QDs were dispersed in hexane for characteristic analysis without any size-selective precipitation. For the synthesis of the ZnSe QDs, the above procedure is exactly followed with the exception of 2 mmol Se powder replacing S powder.

X-ray diffraction (XRD) analysis was employed to characterize the crystallinity of the as-synthesized nanoparticles by a D/max 2400 X Series X-ray diffractometer. The X-ray radiation source, obtained at 40 kV, 100 mA, was Cu Kα, and the scanning speed was 10° min^{-1} at a step of 0.02°. A transmission electron microscopy (a JEOL 2010F TEM operating at 300 KeV) was used to characterize the morphological properties of the ZnS nanoparticles. The UV–vis absorption spectra of the ZnS nanocrystals in hexane were obtained by a JASCO V-570 UV/VIS/NIR Spectrometer in the range of 250–800 nm. The photoluminescence spectra of the ZnS nanocrystals were measured at room temperature by a Fluoromax-4 spectrometer.

3. Results and discussion

As reported in Ref. [31], the nanometer-sized scale of the QDs can confine electrons in a small box and quantize the energy band possessed by bulk materials into discrete energy states. That is to say, the band gap of the semiconducting materials can be tunable to a desired energy through changing the particle size due to the quantization effect and this variability of the band gap can tune its absorption and emission spectra. For a material, its Bohr excitonic radius, R_B, can be given by the following equation [32]:

$$R_B = \varepsilon_\infty \left(\frac{1}{\mu_e} + \frac{1}{\mu_h}\right) a_B \quad (1)$$

where ε_∞ is the high-frequency dielectric constant, μ_e is the electron effective mass, μ_h is the hole effective mass, a_B is the Bohr radius of hydrogen atom, which is 0.105 nm. Taking the ZnS bulk values of $\varepsilon_\infty = 5.7$, $\mu_e = 0.34$, $\mu_h = 0.58$, thus, the Bohr radius of the ZnS nanocrystals can be calculated by Eq. (1) and its value is 2.79 nm. Generally, if the diameter of the nanocrystals is less than its Bohr excitonic radius, there will be quantum confinement effect for the nanocrystal materials, and the band gap shifts toward higher energies, also named "blue-shift". Compared to the bulk materials, there are many new different features for the QDs, such as generating multiple electron–hole pairs per photo as shown in Fig. 1(b), and Fig. 1(a) shows the situation of generating single electron–hole pair per photo.

Fig. 2 shows exclusive XRD patterns of the ZnS QDs synthesized at different synthesis temperatures, which indicate a highly crystalline characteristic of the as-synthesized product. It can be

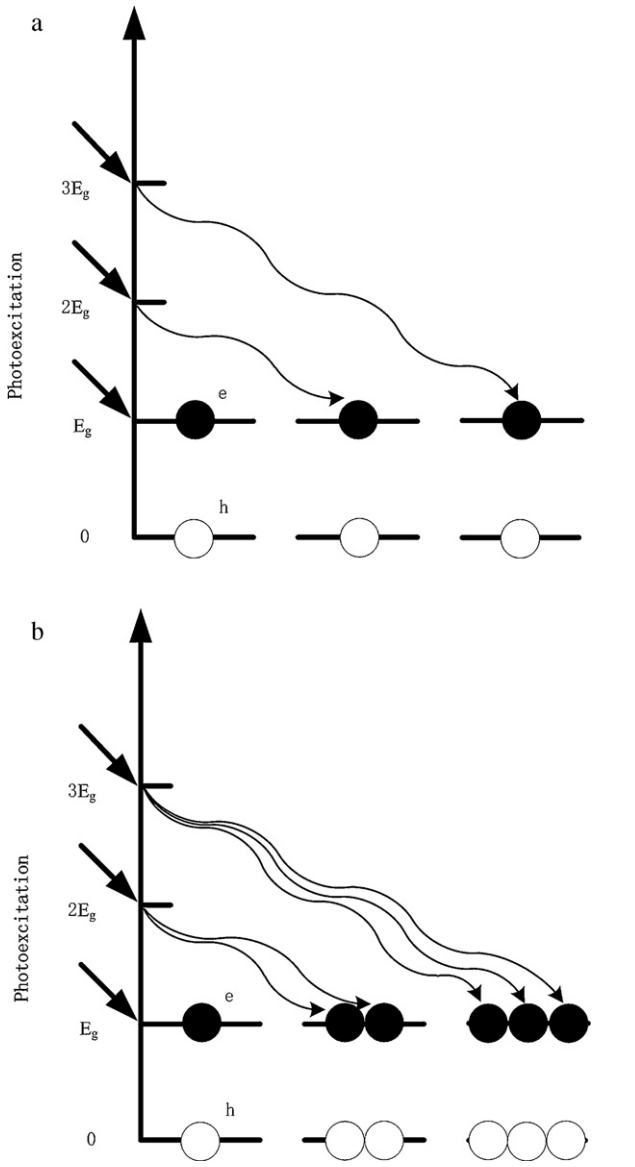

Fig. 1. Schematic diagram of photoexcitation without (a) and with (b) multiple exciton generation.

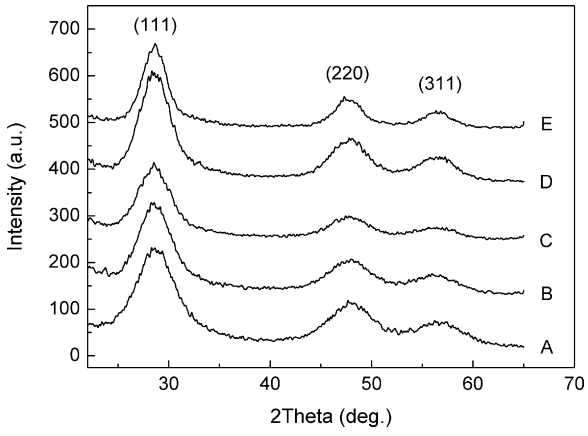

Fig. 2. XRD patterns of the ZnS QDs synthesized at (A): 120 °C; (B): 150 °C; (C): 180 °C; (D): 210 °C; and (E): 240 °C.

Table 1
FWHM and crystal size of the products synthesized at different reaction temperatures.

Temperature (°C)	120	150	180	210	240
FWHM	5.509	4.598	4.408	3.956	3.082
Crystal size (nm)	1.7	2.0	2.1	2.4	3.1

assumed that the S is reduced to S^{2-}, while the oleylamine can be believed to be oxidized. In fact, the oleylamine in our experiment is not only as the reaction solvent and dispersant, but also as the reducing agent in the redox reaction. However, further study is needed to determine the oxidization products of the oleylamine. It can be seen from Fig. 2 for the as-synthesized samples that several main diffraction peaks at 28.65°, 47.60°, and 56.53°, which correspond to the (1 1 1), (2 2 0), (3 1 1) reflection directions, are observed. All these diffraction peaks coincide with their standard bulk crystal structure patterns of the ZnS (JCPDS 05-0566). XRD patterns indicate that the obtained products are the blende ZnS. The diffraction peaks are quite broad, indicating a typical of the crystalline QD material. It can be found that there is few difference between those XRD patterns from the curves *A* to *E* with increasing the synthesis temperature, except for the FWHMs. Actually, the FWHM for the (1 1 1) diffraction peak decreases with the rising of the synthesis temperature, and the precise values are presented in Table 1. Using the Debye-Scherrer formula for the (1 1 1) direction, the crystal size of the as-synthesis ZnS QDs can be calculated and the values are also presented in Table 1. It can be concluded from above these XRD results that the higher synthesis temperature leads to the bigger crystal size, and the ZnS QDs can be easily synthesized at very low temperature. It is also noted in our experiment that the ZnS QDs can be synthesized at 60 °C for 30 min, but the yield of the products with well-dispersed QDs is very low.

The size and morphology of the as-synthesized blende ZnS nanoparticles are characterized by TEM. Fig. 3 shows the TEM images of the nanoparticles synthesized at 240 °C. It can be observed that the size of the ZnS nanocrystals is in a range of 3–4 nm in diameter, which agrees with the crystal size calculated from Debye-Scherrer formula. Fig. 3(a) shows a low-magnification pattern, which reveals very small nanoparticles with a narrow size distribution and no any aggregation is found. Basically, the shape of the nanoparticles is spherical. Fig. 3(b) shows a high-magnification pattern of the as-synthesized nanoparticles, from which the size of the nanoparticles can be seen more clearly. The inset of Fig. 3(b) shows a high-resolution TEM (HRTEM) image of the ZnS specimen synthesized at 240 °C. The visible lattice fringe indicates that the as-prepared ZnS nanocrystals are highly crystalline and the observed lattice spacing is calculated to be ca. 0.31 nm, which matches well to the (1 1 1) plane of the ZnS. The fringe of the nanoparticles is fuzzy, indicating that these nanoparticles are well passivated and protected by the oleylamine.

Fig. 4(a) shows the UV–vis absorption spectra of the colloidal ZnS QDs dispersed in hexane. It can be seen that the absorption shifts to longer wavelengths as the synthesis temperature increases, and a broad shoulder with a long tail extending to longer wavelengths appears between 280 and 310 nm. The inset of Fig. 4(a) shows that a red shift of the absorption edge occurs with the increase of the synthesis temperature, i.e., with the increase of the nanoparticle size. It can be found from Fig. 4(a) that there is no absorption for the as-synthesized ZnS QDs at the wavelength of longer than 335 nm, indicating that the visible and infrared light can completely pass the ZnS and hexane mixture without any attenuation. These results indicate that the as-synthesized ZnS QDs can be used as a window layer to prevent from ultraviolet light and pass the visible and infrared light entirely.

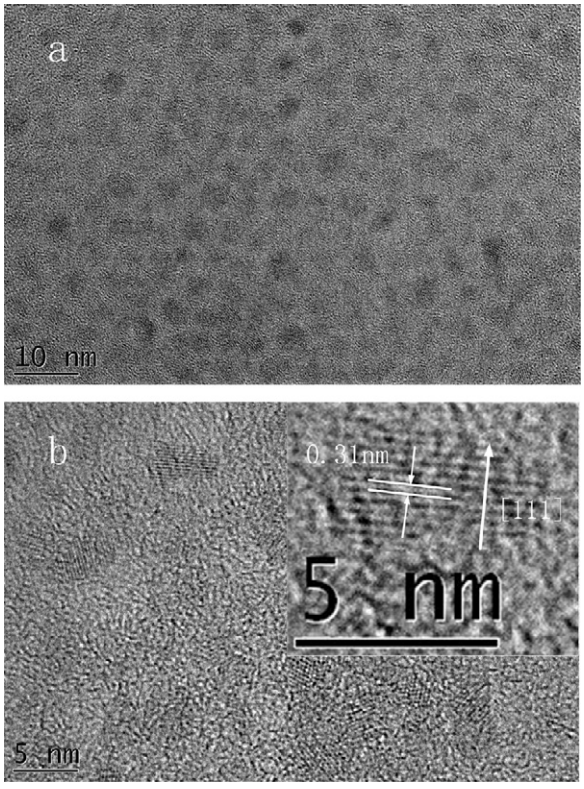

Fig. 3. TEM images of the ZnS nanoparticles synthesized at 240 °C. (a) Low-magnification; (b) high-magnification and HRTEM is shown in the inset.

It is well known that the absorption coefficient (α) is related to the incident photo energy ($h\nu$) by the following equation [33]:

$$\alpha h\nu = A(h\nu - E_g)^m \quad (2)$$

where h is the Planck's constant, ν is the photo frequency, A is a constant, E_g is the band gap, m is the index indicating the type of transition. As one knows, the value of m for direct band gap semiconductor is 1/2, and for indirect band gap semiconductor is 2 [34]. ZnS is a direct band gap semiconductor, therefore $m = 1/2$. Thus, the optical band gap E_g can be obtained from the plot of $(\alpha h\nu)^2$ vs. $h\nu$ as shown in Fig. 4(b). It can be seen that the band gaps of the as-synthesized specimens are 4.16 eV, 4.06 eV, 4.01 eV, 3.99 eV, and 3.90 eV, which correspond to the synthesis temperatures at 120 °C, 150 °C, 180 °C, 210 °C, and 240 °C, respectively. With an extension of the reaction time, the band gap of the as synthesized specimen becomes gradually narrower and shows a decreasing function of the synthesis temperature. The distinct blue-shift of the absorption wavelength of the ZnS specimen indicates that the size of the as-synthesized ZnS in present study is in the quantum confinement region. However, the Bohr excitonic radius calculated by Eq. (1) is 2.79 nm, while the crystal size of the specimen synthesized at 240 °C as presented in Table 1 is 3.1 nm, which is bigger than its Bohr excitonic radius. That is to say, the quantum confinement effect cannot happen for the specimen synthesized at 240 °C and thus contradictory seems to appear. It is probably related to that the value of the Bohr excitonic radius calculated with Eq. (1) is not so exact, whose model is based on the model of hydrogen atom and some predigestion is introduced. These results indicate that the value of the Bohr excitonic radius calculated with Eq. (1) is probably smaller than its real value.

For a spherical particle whose size is smaller than the Bohr radius of the bulk exciton, when the quantum confinement becomes effective, the size dependence of the band gap energy, $E(R)$, can be given

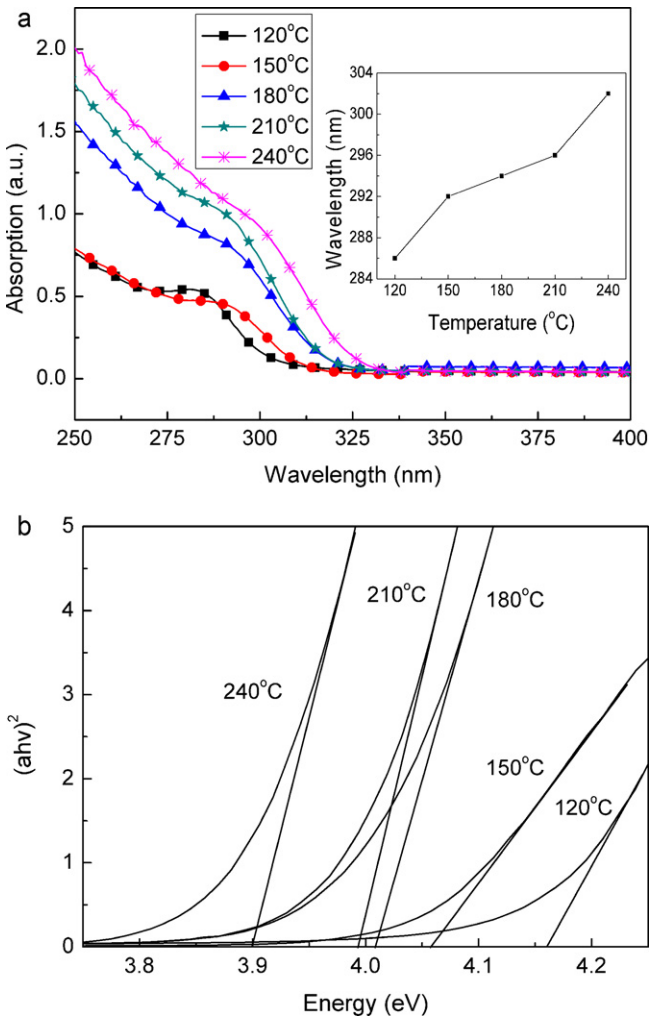

Fig. 4. (a) Optical absorption spectra of the colloidal ZnS QDs synthesized at various temperatures for 30 min. The inset shows the relationship between their absorption peak wavelength and the synthesis temperature. (b) Plots of $(\alpha h\nu)^2$ against photo energy ($h\nu$) for the ZnS QDs specimens synthesized at various temperatures.

by the following effective-mass approximation [35]

$$E(R) = E_g + \frac{\hbar^2\pi^2}{2R^2}\left[\frac{1}{m_e} + \frac{1}{m_h}\right] - \frac{1.786e^2}{\varepsilon R} - \frac{0.124e^4}{\varepsilon^2\hbar^2[1/m_e + 1/m_h]} \quad (3)$$

where R is the particle radius, E_g is the bulk band gap (3.68 eV for ZnS), $\hbar$ is the reduced Planck constant, m_e and m_h are the effective masses of the electron and the hole, respectively, e is the elementary charge, ε is the bulk dielectric constant. Fig. 5 compares the data of the calculated and the experimental (as shown in Fig. 4(b)) band gaps. It shows that the calculated data is bigger than the experimental data and the difference between the calculated data and the experimental data decreases as the crystal size increases. The difference is probably related to the following factors:

a) The assumption of a parabolic energy band in Eq. (3) is inappropriate [35];
b) the values of the band gap are computed with the parameters of the ZnS bulk material to replace the parameters of the ZnS QDs. Actually, the effective mass increases with the decrease of the QDs sizes [36];
c) the crystal size, which is usually slightly smaller than the particle size, is used as the particle size to calculate the band gap, resulting in a larger data.

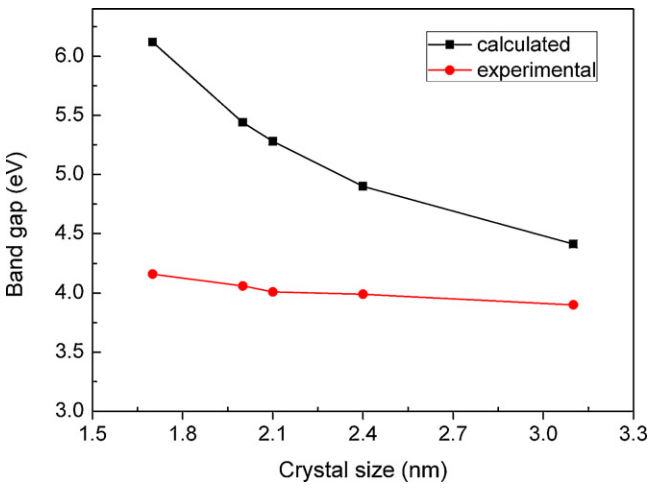

Fig. 5. Size-dependent band gaps of the ZnS QDs obtained by the experiment as shown in Fig. 4 and calculated by Eq. (3).

Furthermore, room temperature photoluminescence (PL) spectra of the as-synthesized ZnS QDs are also measured and shown in Fig. 6(a). The sample synthesized at 120 °C exhibits a broad and strong emission at 389 nm, which dominates the PL spectra, and a very weak emission at 377 nm can be also observed at an excitation

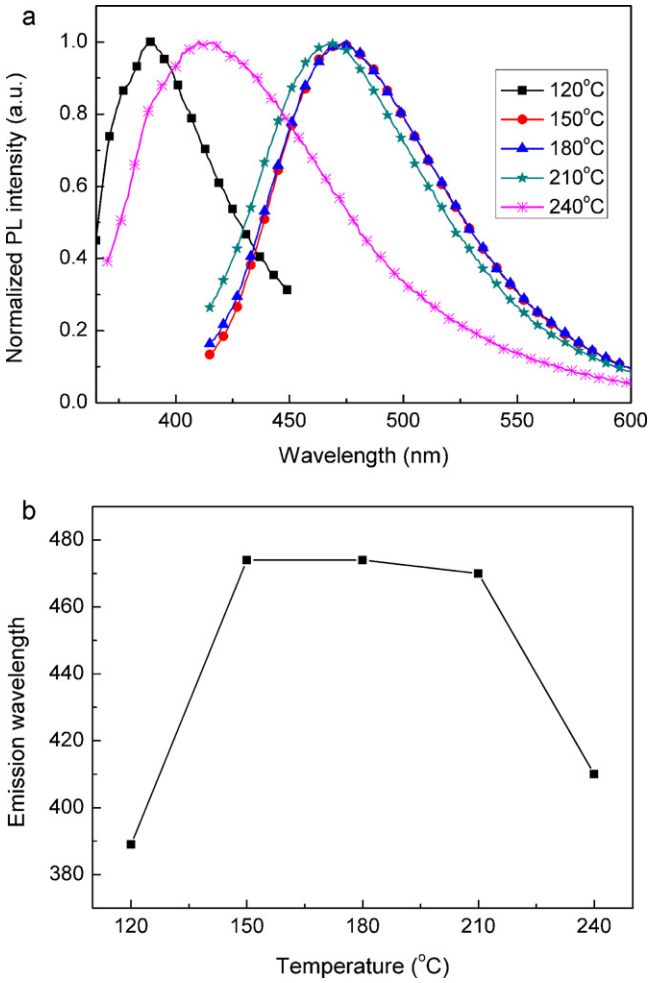

Fig. 6. (a) Normalized PL spectra of the ZnS QDs synthesized at various temperatures; (b) change of the emission wavelength of the specimens with the synthesis temperature.

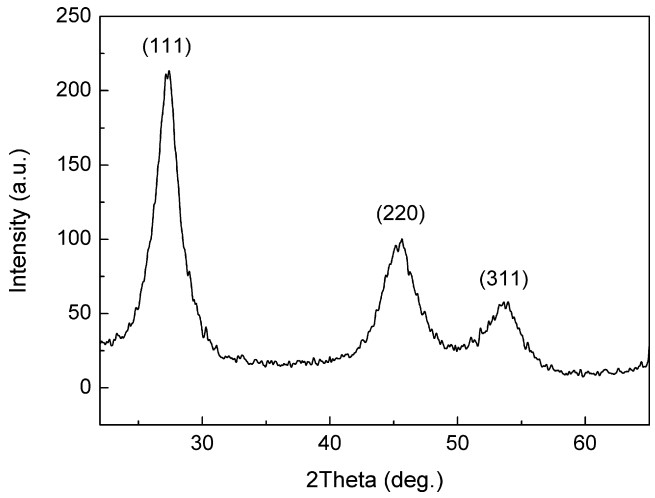

Fig. 7. XRD pattern of the ZnSe nanocrystals synthesized at 180 °C for 30 min.

of 340 nm. The main peak should be assigned to the intrinsic excitation of the ZnS QDs and the weaker emission is probably caused by the crystal defects of the ZnS. Samples synthesized at 150 °C, 180 °C, and 210 °C are excited at 392 nm, 389 nm, and 381 nm, respectively, and exhibit broad and strong emissions at 474 nm, 474 nm, and 470 nm, respectively. There are no other emission peaks besides the main emission peak at about 474 nm or 470 nm, which demonstrates that there are few crystal defects inside these specimens. However, the sample synthesized at 240 °C exhibits a broad and strong emission at 410 nm and also a second very weak emission at about 388 nm at an excitation of 338 nm. The weak emission is still ascribed to the crystal defects of the ZnS QDs. According to the normalized PL spectra, it can be noted that the emission spectra broaden, and the main emission peak first shifts to longer wavelength and then to shorter wavelength as shown in Fig. 6(b) with the increase of the synthesis temperature. When the synthesis temperature increases from 150 °C to 210 °C, the change of the crystal size leads to little change of the emission spectra in shape and intensity. Thus, it is reasonable to predicate that few crystal defects exist in the ZnS QDs synthesized at a temperature from 150 °C to 210 °C.

Fig. 7 shows the XRD pattern of the ZnSe nanocrystals synthesized at 180 °C for 30 min with the same synthesis method. According to the FWHM of the (1 1 1) direction, it is estimated that the crystal size of the ZnSe nanocrystals is 3.6 nm. Its UV–vis absorption spectrum is shown in Fig. 8(a). It can be seen that the absorption peak of the ZnSe nanocrystals is at about 392 nm, which is in the near visible light region. Fig. 8(b) is the pattern of the plots of $(\alpha h\nu)^2$ against photo energy $(h\nu)$ for the ZnSe nanocrystals according to the UV–vis absorption spectrum and it is found that the band gap is 3.01 eV. It can be concluded based on the above results that the present synthesis method is also applicable to synthesize other binary II–VI semiconductor materials.

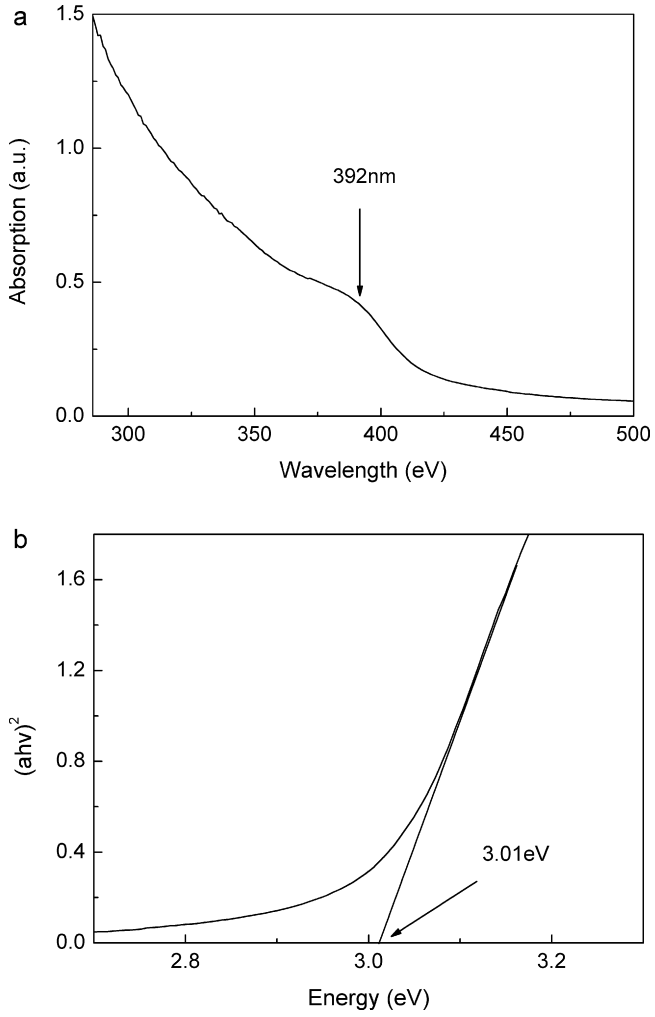

Fig. 8. (a) Optical absorption spectrum of the colloidal ZnSe nanocrystals obtained at 180 °C; (b) plot of $(\alpha h\nu)^2$ against photo energy $(h\nu)$ for the ZnSe nanocrystals synthesized at 180 °C.

4. Conclusions

The ZnS and ZnSe QDs have been successfully synthesized by a facile and novel method. Effects of the solvothermal synthesis temperature on the crystal size, the absorption spectra, and the PL spectra of the examples have been studied. XRD results indicate that the as-synthesized ZnS QDs have a blende structure. The change of the crystal size with the increase of the synthesis temperature has been also studied. It is found that the calculated data based on the energy band is much bigger than the experimental data, but the difference between them is smaller and smaller with the increase of the synthesis temperature. It is also noted that the absorption spectrum of the as-synthesized QDs is related to the particle size and appears a blue-shift. The PL spectra results indicate that the ZnS QDs synthesized at a temperature from 150 °C to 210 °C have a perfect crystal structure and both too high synthesis temperature and too low synthesis temperature lead to the appearance of the crystal defects inside the materials.

Acknowledgments

This work was supported by the Ministry of Science and Technology of China through 863-project under grant 2009AA03Z218, the Major Program of the National Natural Science Foundation of China under Grant No. 90923012, and Xi'an Applied Materials Innovation Fund (XA-AM-200909).

References

[1] M. Bruchez Jr., M. Moronne, P. Gin, S. Weiss, A.P. Alivisatos, Science 281 (1998) 2013–2016.
[2] C.B. Murray, C.R. Kagan, M.G. Bawendi, Annu. Rev. Mater. Sci. 30 (2000) 545–610.
[3] X. Wu, K.W. Li, H. Wang, J. Alloys Compd. 487 (2009) 537–544.
[4] W.C.W. Chan, S. Nie, Science 281 (1998) 2016–2018.
[5] V.L. Colvin, M.C. Schlamp, A.P. Alivisatos, Nature 370 (1994) 354.
[6] V.I. Klimov, A.A. Mikhailovsky, S. Xu, A. Malko, J.A. Hollingsworth, C.A. Leatherdale, H.J. Eisler, M.G. Bawendi, Science 290 (2000) 314–317.

[7] A.Y. Nazzal, L. Qu, X. Peng, M. Xiao, Nano Lett. 3 (2003) 819–822.
[8] W.W. Yu, Y.A. Wang, X. Peng, Chem. Mater. 15 (2003) 4300–4308.
[9] Z. Peng, X. Peng, J. Am. Chem. Soc. 123 (2001) 183–184.
[10] M.E. Mathew, J.C. Mohan, K. Manzoor, S.V. Nair, H. Tamura, R. jayakumar, Carbohydr. Polym. 80 (2010) 442–448.
[11] S.L. Hou, X.Q. Zhang, H.B. Mao, J.Q. Wang, Z.Q. Zhu, W.P. Jing, Phys. Stat. Sol. B 246 (10) (2009) 2333–2336.
[12] Y. He, H.F. Wang, X.P. Yan, Chem. Eur. J. 15 (2009) 5436–5440.
[13] K. Dimos, I.B. Koutselas, M.A. Karakassides, J. Phys. Chem. B 110 (2006) 22339–22345.
[14] S.M. Yang, C.H. Huang, J. Zhai, Z.S. Wang, L. Jiang, J. Mater. Chem. 12 (2002) 1459.
[15] L.J. Diguna, Q. Shen, J. Kobayashi, T. Toyoda, Appl. Phys. Lett. 91 (2007) 023116.
[16] L.W. Chong, H.T. Chien, Y.L. Lee, J. Power Sources 195 (2010) 5109–5113.
[17] K.L. Choy, B. Su, Thin Solid Films 388 (2001) 9–14.
[18] J. Wang, H. Han, J. Colloid Interface Sci. 351 (2010) 83–87.
[19] T. Wang, J. Wang, Y. Zhu, F. Xue, J. Cao, Y. Qian, J. Phys. Chem. Solids 71 (2010) 940–945.
[20] M. Zelner, H. Minti, R. Reisfeld, H. Cohen, Y. Feldman, S.R. Cohen, R. Tenne, J. Sol–Gel Sci. Technol. 20 (2001) 153–160.
[21] E.S.F. Neto, N.O. Dantas, S.W. da Silva, P.C. Morais, M.A.P. da Silva, J. Raman Spectrosc. 41 (2010) 1302–1305.
[22] N.O. Dantas, A.D. Silva, S.W. da Silva, P.C. de Morais, M.A. Pereira-da-Silva, G.E. Marques, Chem. Phys. Lett. 500 (2010) 46–48.
[23] Y. Yin, A.P. Alivisatos, Nature 437 (2005) 664.
[24] J. Luo, D. Qu, A. Tikhonov, J. Bohn, S.A. Asher, J. Colloid Interface Sci. 345 (2010) 131–137.
[25] X.C. Jiang, Y. Xie, J. Lu, L.Y. Zhu, W. He, Y.T. Qian, Chem. Mater. 13 (2001) 1213.
[26] W.T. Yao, S.H. Yu, Q.S. Wu, Adv. Funct. Mater. 17 (2007) 623–631.
[27] Y.W. Zhao, Y. Zhang, H. Zhu, G.C. Hadjipanayis, J.Q. Xiao, J. Am. Chem. Soc. 126 (2004) 6874.
[28] J. Yang, C. Xue, S.H. Yu, J.H. Zeng, Y.T. Qian, Angew. Chem. Int. Ed. 41 (2002) 4697.
[29] Y.C. Li, X.H. Li, C.H. Yang, Y.F. Li, J. Phys. Chem. B 108 (2004) 16002.
[30] L. Li, T.J. Daou, I. Texier, T.T.K. Chi, N.Q. Liem, P. Reiss, Chem. Mater. 21 (2009) 2422–2429.
[31] A.P. Alivisatos, J. Phys. Chem. 100 (1996) 13226.
[32] R.S. Knox, Theory of Excitons; Solid State Physics Supplement 5 , Academic Press, NY, 1963.
[33] J.I. Pankove, Optical Processes in Semiconductor , Dover, NY, 1971, 34–44.
[34] P. Guha, D. Das, A.B. Maity, D. Ganguli, S. Chaudhuri, Sol. Energy Mater. Sol. Cells 80 (2003) 115.
[35] Y. Wang, N. Herron, J. Phys. Chem. 95 (1991) 525–532.
[36] A. Henglein, Chem. Rev. 89 (1989) 1861.